

# Mesenchymal Stem Cell-Derived Extracellular Vesicles Protect Rat Nucleus Pulposus Cells from Oxidative Stress

CARTILAGE  
2024, Vol. 15(3) 328–344  
© The Author(s) 2023  
DOI: 10.1177/19476035231172154  
journals.sagepub.com/home/CAR  


Sobia Ekram<sup>1</sup>, Shumaila Khalid<sup>1</sup>, Faiza Ramzan<sup>1</sup>, Asmat Salim<sup>1</sup>,  
Imtiaz Bashir<sup>2</sup>, Marie Christine Durrieu<sup>3</sup>, and Irfan Khan<sup>1</sup> 

## Abstract

**Background.** Oxidative stress (OS) is mainly associated with the pathogenesis of intervertebral disc (IVD) degeneration; it causes nucleus pulposus cells (NPCs) to undergo senescence and triggers autophagy and apoptosis. This study aims to evaluate the regeneration potential of extracellular vesicles (EVs) derived from human umbilical cord-mesenchymal stem cells (hUC-MSCs) in an *in vitro* rat NPC-induced OS model. **Design.** NPCs were isolated from rat coccygeal discs, propagated, and characterized. OS was induced by hydrogen peroxide (H<sub>2</sub>O<sub>2</sub>), which is confirmed by 2,7-dichlorofluorescein diacetate (H<sub>2</sub>DCFDA) assay. EVs were isolated from hUC-MSCs and characterized by analyzing the vesicles using fluorescence microscope, scanning electron microscope (SEM), atomic force microscope (AFM), dynamic light scattering (DLS), and Western blot (WB). The *in vitro* effects of EVs on migration, uptake, and survival of NPCs were determined. **Results.** SEM and AFM topographic images revealed the size distribution of EVs. The phenotypes of isolated EVs showed that the size of EVs was 403.3 ± 85.94 nm, and the zeta potential was -0.270 ± 4.02 mV. Protein expression analysis showed that EVs were positive for CD81 and annexin V. Treatment of NPCs with EVs reduced H<sub>2</sub>O<sub>2</sub>-induced OS as evidenced by a decrease in reactive oxygen species (ROS) levels. Co-culture of NPCs with Dil-labeled EVs showed the cellular internalization of EVs. In the scratch assay, EVs significantly increased NPC proliferation and migration toward the scratched area. Quantitative polymerase chain reaction analysis showed that EVs significantly reduced the expression of OS genes. **Conclusion.** EVs protected NPCs from H<sub>2</sub>O<sub>2</sub>-induced OS by reducing intracellular ROS generation and improved NPC proliferation and migration.

## Keywords

extracellular vesicles, human umbilical cord, mesenchymal stem cells, nucleus pulposus, oxidative stress, intervertebral discs, reactive oxygen species

## Introduction

The use of extracellular vesicles (EVs) is a cutting-edge regenerative medicine approach that has revolutionized traditional therapeutic modalities by advancing the cell-free therapeutic paradigm.<sup>1</sup> EVs, along with secretory vesicles, invaginate from parent cells *via* the endosomal route in normal physiological and pathological conditions, mediating intracellular signaling for cell survival and cell function. EVs typically range from 30 to 1,000 nm in diameter.<sup>2</sup> They are released in biological fluids, including blood,<sup>3,4</sup> amniotic fluid,<sup>5</sup> synovial fluid,<sup>6</sup> saliva,<sup>7</sup> and other body fluids.<sup>8</sup> The functional mechanism of EVs is accomplished *via* body fluids.<sup>9</sup> EVs can be isolated from the supernatant of cell culture medium *in vitro*.<sup>10</sup> Biological components of macromolecules mainly carried by EVs in intercellular communications

are lipids (phosphatidylserine, sphingomyelin, and cholesterol),<sup>11</sup> proteins,<sup>12</sup> and nucleic acids that perform various biological functions.<sup>13</sup> Besides modulating the phenotypes of targeted cells, EVs also carry messenger ribonucleic acids

<sup>1</sup>Dr. Panjwani Center for Molecular Medicine and Drug Research, International Center for Chemical and Biological Sciences, University of Karachi, Karachi, Pakistan

<sup>2</sup>University of Bordeaux, CNRS, Bordeaux INP, CBMN, UMR 5248, Pessac, France

<sup>3</sup>Zainab Panjwani Memorial Hospital, Karachi, Pakistan

### Corresponding Author:

Irfan Khan, Dr. Panjwani Center for Molecular Medicine and Drug Research, International Center for Chemical and Biological Sciences, University of Karachi, Karachi 75270, Pakistan.

Email: khan@iccs.edu



(mRNAs),<sup>14</sup> microRNAs,<sup>15</sup> and long non-coding RNAs,<sup>16</sup> which efficiently play key roles in gene regulation *via* chromatin modification, transcription activation, transcription, translation, posttranslational regulation, and their interaction with deoxyribonucleic acid (DNA), RNA, and proteins<sup>17</sup> to maintain the pathophysiology of biological processes.<sup>18</sup> The nanosize of EVs holds various advantages such as biocompatibility, transport through the cell membrane, intrinsic properties for target cells, and long-term stability.<sup>19</sup>

The intervertebral disc (IVD), an avascular structure located between adjacent vertebral bodies, is responsible for the organization of spinal support and kinematics.<sup>20</sup> There are 3 basic cartilage-like tissues present in an IVD: nucleus pulposus (NP), annulus fibrosus (AF), and cartilaginous endplate (CEP).<sup>21</sup> Human NP is made up of 2 types of cells: chondrocyte-like cells and vacuolated notochord cells.<sup>22</sup> Intervertebral disc degeneration (IVDD) is a major health dilemma characterized by numerous pathological conditions, clinically corresponding to low back pain (LBP), IVD herniation, spinal deformities, and spinal canal stenosis.<sup>23</sup> Long-term disabilities caused by these spinal disorders are the leading cause of economic burden.<sup>24</sup> The prevalence of IVDD has a multifactorial and complex etiology mainly contributed by mechanical stress, aging, infection, smoking, trauma, and heredity.<sup>25</sup> Currently, there are no effective therapies available to treat IVDD due to a limited understanding of the molecular mechanisms, as the pathogenesis of IVDD is linked to the loss of notochordal cells and chondrocyte cells of the NP.<sup>22</sup> Mechanistically, IVDD is characterized by the breakdown of the extracellular matrix (ECM) with increased expression of ECM-degrading enzymes followed by loss of water and upregulation of proinflammatory cytokines, *interleukin (IL)-1* and *tumor necrosis factor-alpha (TNF- $\alpha$ )*, leading to pathophysiological conditions and an imbalance in homeostasis.<sup>26</sup>

Furthermore, significantly high expression of oxidative stress (OS) marker was initiated by reactive oxygen species (ROS) such as *TNF- $\alpha$* , *cyclooxygenase-2 (COX-2)*, *matrix metalloproteinase-3 (MMP-3)*, advanced glycation end products (AGEs), carboxymethyl-lysine, and peroxynitrite, which eventually aggravate IVDD.<sup>27</sup> The generation of ROS plays a critical role in regulating IVD cell signaling and viable cells present in the IVD microenvironment, which also contributes to the pathogenesis of IVDD; OS in IVDs eventually compromises extracellular mechanical functions.<sup>28</sup> Additional therapies to prevent ROS production as well as IVD-induced cell senescence would provide an alternative approach to treat IVDD, targeting OS.<sup>29</sup> An avascular arrangement of IVDs mainly depends on mitochondrial integrity and biogenesis. It has been established that mitochondrial dysfunction is the cause of NP cell death and IVDD.<sup>30</sup> A study observed that increased NP cell degradation due to autophagic cell death could be rescued by

reducing the intracellular generation of ROS; thus, diminishing OS may treat IVDD.<sup>31</sup> Many strategies, including tissue engineering, gene therapy, and cell-based therapy, as well as surgical and pharmacological interventions, are currently being used to treat IVDD.<sup>32</sup> Mesenchymal stem cell (MSC)-based treatment for IVDD has shown promising effects; however, there have been biological and ethical concerns for long-term maintenance of these cell-based procedures due to their low cell survival rate, targeted engraftment, regulation of cell differentiation, cell viability, mutations, and risks of tumorigenesis.<sup>33</sup> It is reported that stem cell-derived EVs play a role in regeneration while lowering the risks associated with a cell-based therapeutic approach to treating IVDD.<sup>34</sup>

In this study, *ex vivo* isolation of human umbilical cord (hUC) tissue-derived MSCs were used to produce EVs, which promoted MSC migration and differentiation into NP-like cells, reducing oxidative damage and regulating endogenous IVD repair and regeneration. Eventually, it can be used to effectively ameliorate the IVDD prognosis. The critical aspects of naive EVs for bypassing biological rejection of recipient cell organization are due to their nano-scale size, stability, and low immunogenicity, which require optimized protocols for EV isolation and characterization to impact the progress and understanding of the process of IVDD.<sup>35</sup>

## Methods

### Ethical Statement

The following experimental procedures were approved by the Institutional Animal Care and Use Committee (IACUC) of the International Center for Chemical and Biological Sciences, University of Karachi under the animal study protocol approval no. 2017-0051. All animal procedures were performed in compliance with the international guidelines and regulations for the care and use of laboratory animals. All experimental procedures using human samples were approved by the Ethical Committee for Human Subjects.

### Rat Nucleus Pulposus Cell Isolation and Culture

The NP regions were extracted from adult male Wistar rats ( $n = 10$ ), as described earlier by Risbud *et al.*<sup>36</sup> Wistar rats weighing 250 to 300 g and aged 2 to 4 months were sacrificed by injecting an overdose of sodium pentobarbital (150 mg/kg), followed by decapitation, following IACUC protocols. The animals were sacrificed as previously reported,<sup>37</sup> and their tails were harvested in an aseptic manner to obtain the coccygeal vertebrae. Furthermore, the attached ligamentous and muscular tissues were also removed, and the central gelatinous NP tissues were immediately isolated from the coccygeal discs. The isolated NP tissues were

transferred to a tube and washed with phosphate-buffered saline (PBS). The obtained NP tissues were transferred into a T-25 flask containing Dulbecco's modified eagle's medium (DMEM) (Gibco) supplemented with 10% fetal bovine serum (FBS) (ThermoFisher Scientific, USA), 1% penicillin/streptomycin (Gibco), 4 mM L-glutamine (Gibco), and 1 mM sodium pyruvate (Gibco), termed as complete DMEM, and incubated at 37 °C and maintained at 5% carbon dioxide (CO<sub>2</sub>). The culture media was replaced with fresh media after every 3 days. After 5 to 10 days, cell attachment to the flask surface was observed. At 70% to 80% confluence, cells were detached and subcultured. Passage 2 to 4 (P<sub>2</sub>-P<sub>4</sub>) cells were used in the study.

### Colony-Forming Unit Assay

One thousand cells were seeded in a 6-well plate for the colony-forming unit (CFU) assay and incubated in complete DMEM. The medium was changed every third day. After 2 weeks of incubation, cells were rinsed twice with PBS, fixed with 4% paraformaldehyde (PFA), and stained with 0.1% Crystal violet for 15 minutes. For counting, clusters of 500 cells were considered as a colony. Data were analyzed by Statistical Package for the Social Sciences (SPSS) software program, version 21.0.

### Cell Growth Analysis

The population doubling level (PDL) was analyzed to investigate the proliferation of nucleus pulposus cells (NPCs) between P<sub>0</sub>, P<sub>1</sub>, and P<sub>2</sub> using the given formula according to a previously reported method<sup>38</sup>:

$$PDL = 3.32 * [\log(\text{final cell number}) - \log(\text{initial cell number})].$$

The sum of all PDL passages yielded the cumulative population doubling level (cPDL).<sup>39</sup> The rate of growth of NPCs was investigated using the following equation based on the population doubling rate (PDR) in each sub-cultivation<sup>40</sup>:

$$PDR = \text{Population doubling rate} / \text{Culture time in days.}$$

### Immunofluorescence Analysis of Rat NPCs

Cells isolated from rat IVDs at P<sub>3</sub> were seeded in chambered glass slides (Iwaki, Japan) and fixed with 4% PFA. After permeabilization with 0.1% Triton X-100, cells were rinsed with PBS and blocked with 2% bovine serum albumin (BSA) and 0.1% Tween 20 in PBS for 1 hour at 37 °C. Then, the slides were incubated overnight at 4 °C with the following antibodies: SRY-box transcription factor 9

(SOX-9), transforming growth factor-beta 1 (TGF-β1), transforming growth factor-beta 2 (TGF-β2), aggrecan (ACAN), collagen 1 (COL-1), and STRO-1 at recommended dilutions. Following a PBS wash, cells were incubated with Alexa Fluor 488 secondary antibodies at room temperature (RT) for 1 hour at 1:200 dilution. Alexa flour 546-labeled phalloidin (1:200 dilution) was used to stain cytoskeletal protein F-actin. The nuclei were stained with 0.5 ng/ml 4',6-diamidino-2-phenylindole (DAPI) for 10 minutes, and glass slides were mounted with an aqueous mounting medium. As controls, NPCs treated with DAPI and isotype-secondary antibodies were used. Images were captured under a fluorescence microscope (NiE; Nikon). The images were analyzed and processed using NIS Element and Adobe Photoshop software.

### OS Induction

To induce OS, NPCs were seeded in 96-well plates and treated with 10 to 1,000 μM H<sub>2</sub>O<sub>2</sub> solution (Merck) for 1 to 24 hours. OS was assessed by morphological changes and 2,7-dichlorofluorescein diacetate (H<sub>2</sub>DCFDA) assay (Abcam). H<sub>2</sub>DCFDA is oxidized into fluorescent 2,7-dichlorofluorescein (DCF) in the presence of intracellular ROS. NPCs were treated in triplicate with a 20-μM working solution of H<sub>2</sub>DCFDA dye and incubated at 37 °C in the dark for 30 minutes. The relative fluorescence unit (RFU) was measured at 485 and 535 nm wavelengths using a microplate reader (Varioskan LUX).

### Isolation of hUC-MSCs and EVs

The hUC tissues were obtained from human subjects after their informed consent. MSCs were isolated from hUC tissue as previously reported.<sup>37</sup> EVs were isolated from MSC-conditioned medium using a differential centrifugation protocol as previously described by Konoshenko *et al.*<sup>41</sup> Briefly, MSCs were grown in complete DMEM to attain 80% to 90% confluence. The medium was replaced with serum-free DMEM, and cells were incubated for 48 hours at 37 °C in 5% CO<sub>2</sub>. After incubation, the conditioned media was collected to obtain a substantial amount of EVs and centrifuged at 500g for 10 minutes, followed by 800g for 10 minutes to eliminate the cell pellet. The supernatant was collected, and tubes were centrifuged at 2,000g for 20 minutes, followed by 2,000g for 30 minutes to remove cellular debris. The pellet was discarded at every step, and all centrifugations were carried out at 4 °C. Cell-free supernatants were transferred into new falcon tubes and centrifuged at 15,000g for 30 minutes at 4 °C. The EV pellet was harvested and washed with sterile PBS. The purified EVs were quantified by Bradford protein assay and dissolved in 2x radioimmunoprecipitation assay (RIPA) or cell lysis buffer for protein and RNA isolation, respectively.

### Characterization of hUC-MSC-Derived EVs

EVs were characterized based on size and morphology using fluorescence microscope, scanning electron microscope (SEM), atomic force microscope (AFM), dynamic light scattering (DLS), and Western blot (WB).

### Labeling and Imaging of hUC-MSC-Derived EVs

Human umbilical cord-mesenchymal stem cell (hUC-MSC)-derived EVs were labeled with lipophilic cationic membrane-labeling red fluorescent DiI dye (Invitrogen) as per the manufacturer's protocol. Briefly, EVs were treated with 5  $\mu$ l of 10  $\mu$ M DiI-labeling dye in 1 ml serum-free medium and incubated for 5 minutes at 37 °C in 5% CO<sub>2</sub>. EV suspension was centrifuged at 15,000g for 30 minutes at 4 °C. DiI-labeled EVs were observed under a fluorescence microscope (Ti2; Nikon, Japan). All images were captured with NIS-Elements AR software.

### Processing for SEM

EVs were fixed with 4% PFA for 10 minutes, seeded on glass coverslips, and air-dried. A 15-nm conductive gold coating was deposited by the auto-fine coating chamber (JEC-3000FC) to impede charging and strengthen the secondary electron signal. The program was set at 20 mA current for 30 seconds, and images were captured under SEM (JSM-IT 100 SEM; Jeol, Japan). Images were captured and analyzed.

### Processing for AFM

EVs were resuspended in 1:10 dilution of PBS and coated with a freshly cleaved mica sheet and incubated at 37 °C overnight. Next day, scanning measurements in the air were carried out using silicon nitride probes by AFM (Agilent Technologies). Image processing was done using Pico View 1.12.2 software.

### Processing for DLS

EVs were resuspended in 1 ml of sterile PBS and analyzed using DLS instrument for hydrodynamic size distribution and number. Furthermore, zeta potential was measured to determine the stability and integrity of EVs using the Zetasizer Nano ZS system version 7.12 (MAL1160489; Malvern Instruments, Malvern, UK) according to the manufacturer's instructions.

### WB Analysis

hUC-MSCs and EVs were lysed in 2x RIPA buffer with 1 mM phenylmethylsulfonyl fluoride (PMSF) and 10 mM

Na-pyrophosphate. Lysates were incubated on ice for 10 minutes and sonicated twice for 15 seconds, followed by centrifugation for 15 minutes at 16,000g. The aqueous phase was collected and stored at -80 °C. Following denaturation at 95 °C for 10 minutes, the protein was separated on 12% sodium dodecyl sulfate-polyacrylamide gel electrophoresis (SDS-PAGE), followed by transfer of the gel bands to a polyvinylidene fluoride (PVDF) membrane (Immobilin-P; Millipore). PVDF membranes were incubated overnight at 4 °C with anti-CD81 (MA5-13548; Invitrogen) and anti-annexin V (PA5-27872; Invitrogen) solutions (1:100 and 1:500 dilutions, respectively) after blocking with 5% BSA in Tris buffer saline Tween-20 (TBST).<sup>42</sup> Subsequently, the membranes were rinsed 5 times in TBST and incubated for 2 hours with horseradish peroxidase (HRP)-conjugated secondary antibody (1:1,000 dilution) (7076; Cell Signaling, USA). Membranes were washed with TBST 5 times and developed using a chemiluminescence substrate.

### Evaluation of the Effect of hUC-MSC-Derived EVs on NPCs

ROS analysis, fluorescence microscopy, quantitative polymerase chain reaction (qPCR), and a scratch wound healing assay were performed to investigate the effects of EVs on OS, EV internalization, and NPC migration.

### ROS Analysis

For ROS induction, NPCs in the exponential phase were treated with an optimized concentration (200  $\mu$ M) of H<sub>2</sub>O<sub>2</sub> for 2 hours in chamber slides. EVs were added to the control and OS-induced NPCs for 48 hours, and NPCs were incubated with 20  $\mu$ M H<sub>2</sub>DCFDA for 30 minutes. After incubation, the dye was removed, cells were rinsed once with PBS, and fixed with 4% PFA at RT for 15 minutes. The cytoskeleton of NPCs was stained with Alexa Fluor 546-labeled phalloidin at a 1:200 dilution for 1 hour. Nuclei were costained with DAPI for 5 minutes at RT. The images were acquired with a fluorescence microscope, and the mean fluorescence intensity (MFI) of cells was measured by the ImageJ software (NIH, Bethesda, MD, USA). MFI of cells was measured in triplicate in each analysis and plotted with GraphPad Software.

### DiI Labeling and Cellular Uptake of EVs

EVs were incubated with 5  $\mu$ l of lipophilic cationic DiI membrane-labeling dye in serum-free DMEM for 5 minutes in the dark at 37 °C. After incubation, the dye was removed by replacing it with 5 ml of DMEM and then centrifuged twice at 15,000g for 30 minutes at 4 °C to wash the EV pellet. Finally, EVs were resuspended in DMEM.

**Table 1.** List of Primers Used in Quantitative Polymerase Chain Reaction Analysis.

Gene	Forward (5'-3')	Reverse (5'-3')
<i>rNRF2</i>	5'-GAC AGC TGT AGT CCA CAT TTC CT-3'	5'-AGC TTT ACA CAG GGA CAG ATC AC-3'
<i>rSOD1</i>	5'-GTG GCC AAT GTG TCC ATT GAA G-3'	5'-CAA TCC CAA TCA CAC CAC AAG C-3'
<i>rSOD2</i>	5'-CAG ATT GCC TGC TCT AAT-3'	5'-CAA GAG CAG CTC ACA CCA AGT-3'
<i>rPRDX1</i>	5'-CAA AGC CAC GGC TGT TAT GC-3'	5'-TGG GTC CCA ATC CTC CTT GT-3'
<i>rPRDX2</i>	5'-TGT GAC TAA AAG CTT GTC CCA GAA T-3'	5'-TGT TTG GAG AAG TAT TCC TTG CTG T-3'
<i>rPRDX3</i>	5'-AAT GCA TTG TGG TCT GGT TC-3'	5'-CAG CAC ACC GTA GTC TCG G-3'
<i>rPRDX4</i>	5'-CGC TAC CCG CGA CGA CTC-3'	5'-AGT CCT TTG AGA TCT GAT GG-3'
<i>rGPX1</i>	5'-TTC CCG TGC AAT CAG TTC GG-3'	5'-TCC AGG TGT CGT TGC GG-3'
<i>rGPX3</i>	5'-CTC GGA GAT TCT GTC CAC TCT CA-3'	5'-CCG TTC ACG TCC CCT TTC T-3'

DiI-labeled EVs were added to normal and OS-induced NPCs for 48 hours at 37 °C. Following a PBS wash, cells were fixed with 4% PFA and stained with phalloidin labeled Alexa Fluor 488 (1:200) for 1 hour. Cells were treated with DAPI (0.5 ng/ml) for 10 minutes to stain the nuclei. Cellular internalization of EVs was observed under a fluorescence microscope.

### Scratch Assay

NPCs were seeded at a density of  $0.24 \times 10^6$  cells per well of a 6-well plate for 24 hours. A scratch was induced using a 100- $\mu$ l sterile micropipette tip in each well containing normal NPCs. NPCs were then rinsed with PBS before being subjected to OS (200  $\mu$ M, 2 hours). One group of oxidized NPCs was treated with EVs. Images were taken using a phase contrast microscope at 0 to 24 hours following treatment. The area of the scratch was measured using ImageJ software.

### qPCR Analysis for Gene Expression

The expression analysis of OS-responsive genes (*NRF2*, *SOD1*, *SOD2*, *PRDX1*, *PRDX2*, *PRDX3*, *PRDX4*, *GPX1*, and *GPX4*) was performed in normal NPCs, OS-induced NPCs, and OS-induced NPCs treated with EVs for 48 hours. NPCs were washed with PBS, and RNA was isolated using Trizol reagent (Invitrogen) as previously described.<sup>40</sup> The concentration of the isolated RNA was determined by a NanoDrop® Lite spectrophotometer (ThermoFisher Scientific) at 260 nm. The absorbance ratios of 260:280 and 230:260 confirmed the integrity and purity of the RNA. One microgram of RNA was used for first-strand complementary DNA by the RevertAid First-Strand cDNA Synthesis Kit (ThermoFisher Scientific). Specific primers were designed to detect OS-related markers as listed in Table 1. qPCR amplification was performed in triplicate in a 96-well plate using qPCR master mix (A600A; Promega) using CFX96

Touch™ Real-Time PCR Detection System (CFX96; Bio-Rad). The target transcriptional level was determined using the 2-fold  $2^{-\Delta\Delta C_t}$  method and normalized with beta-actin.

### Statistical Analysis

For statistical data analysis, SPSS software version 21.0 (IBM; SPSS, Statistics, USA) was used. Prism version 8.0 was used to plot the graphs (GraphPad Software, USA). All values are presented as mean  $\pm$  standard deviation (SD) from triplicate values. In case of more than 2 groups, analysis of variance (ANOVA) with the Bonferroni *post hoc* multiple comparisons test was used. A  $P < 0.05$  value was considered statistically significant. Thus, each value indicates mean  $\pm$  SD; \* $P < 0.05$ , \*\* $P < 0.01$ , and \*\*\* $P < 0.001$ .

## Results

### NPC Morphology and Growth

NPCs were successfully isolated from the coccygeal region of rat IVD tissues by the explant culture method. Freshly isolated NPCs proliferated rapidly with clonal expansion and were typically arranged in a honeycomb-like structure after 7 days of culture. Isolated NPCs achieved approximately 80% confluence after a week of culture. NPCs at passage zero had an isodiametric appearance that changed to a monolayer with a spindle-shaped morphological appearance as cells progressed through higher passages (Fig. 1A).

### Colony-Formation Unit

Crystal violet staining revealed that NPCs were arranged as colonies. Five hundred cells per cluster were considered a colony, showing that NPCs exhibit better colony-forming efficiency (Fig. 1B).

### Population Doubling Time

NPCs proliferated rapidly as the number of passages increased from  $P_0$  to  $P_2$ . At  $P_2$ , the PDL for NPCs was nearly  $16.02 \pm 0.02$  days, longer than for NPCs at  $P_0$  (Fig. 1C). However, the PDR of cells at  $P_1$  and  $P_2$  showed a higher growth rate than NPCs at  $P_0$  (Fig. 1D). The difference between these passages was significant ( $P < 0.05$ ).

### Features of Immunocytochemical Analysis

The presence of specific NPC proteins or surface antigens was identified by immunocytochemical staining. NPCs showed positive expression of chondrogenic markers SOX-9, TGF- $\beta$ 1, TGF- $\beta$ 2, ACAN, and COL-1, while STRO-1, an MSC-specific antigen, was not expressed (Fig. 1E). Alexa Fluor 546-labeled phalloidin was used to stain the cytoskeleton. DAPI and Alexa Fluor 488 isotype were included as a control group.

### ROS Measurement under OS In Vitro

$P_2$  NPCs exposed to  $H_2O_2$  at concentrations ranging between 10 and 1,000  $\mu$ M showed rounded and shrunken NPCs with damaged cellular matrix around their edges and condensed nuclei at higher concentrations. There is no apparent change in morphology at 1 hour post OS. As the exposure time extended to 24 hours, the majority of the cells showed a thread-like matrix containing condensed nuclei. OS induced by  $H_2O_2$  leads to ROS generation *in vitro*.  $H_2DCFDA$  is a non-fluorescent compound that disperses into cells and becomes fluorescent once it interacts with ROS inside the cells.  $H_2DCFDA$  analysis showed that  $H_2O_2$  significantly increased the ROS level in a concentration and time-dependent manner when compared with the control group (Fig. 2).

### Characterization of hUC-MSCs

MSCs isolated from hUC tissue showed fibroblast-like, spindle-shaped morphology. MSCs showed positive expression of CD29, CD73, CD105, CD117, STRO-1, and vimentin and negative expression of hematopoietic markers CD45 and HLA-DR (Fig. 3A). Flow cytometric analysis also showed positive expression of surface markers CD90, CD44, CD105, and CD73, compared with control, confirming MSCs in the hUC-derived cell population (Fig. 3B). Successful differentiation of hUC-derived cells into osteogenic, chondrogenic, and adipogenic lineages also confirmed the presence of MSCs in culture (Fig. 3C).

### Characterization of hUC-MSC-Derived EVs

EVs isolated by differential centrifugation technique were characterized by phase contrast microscope. Purified EVs

labeled with the DiI dye were visualized using fluorescence microscope (Fig. 4A). SEM at 2,000x magnification revealed rounded molecules with different diameters varying from 0.300 to 0.800  $\mu$ m (Fig. 4B). AFM also revealed the size distribution of EVs through topographic images (Fig. 4C). DLS showed that the size of EVs was  $403.3 \pm 85.94$  nm and the  $z$ -potential was  $-0.270 \pm 4.02$  mV (Fig. 4D). Positive expression of CD81 and annexin V from total protein extract revealed that the isolated population comprises pure EVs (Fig. 4E).

### EVs Inhibit ROS Production

To analyze ROS production, fluorescence intensity of DCF in NPCs was quantified. OS induction by 200  $\mu$ M  $H_2O_2$  for 2 hours increased the fluorescence intensity in NPCs, which indicates the production of ROS. Conversely, treatment of hUC-MSC-derived EVs markedly reduced the level of DCF fluorescence before and after OS induction, respectively (Fig. 5). These outcomes suggested that ROS accumulation was implicated in  $H_2O_2$ -induced OS, and EVs reduced the ROS level in NPCs.

### Internalization of EVs by NPCs

The internalization of hUC-MSC-derived EVs into NPCs was observed using DiI-labeled EVs, added to the normal and OS-induced NPCs for 48 hours. A highly significant correlation was observed between OS and an increase in EV uptake by NPCs that were distributed into the cytoplasm. When compared with normal NPCs, EV uptake increased under OS. These results indicate that hUC-MSC-derived EVs were internalized by the NPCs (Fig. 6).

### EVs Promote NPC Migration

The scratch assay showed that EVs improved NPC migration toward the scratched area. EVs after 24 hours of treatment enhanced NPC migration; NPCs migrated faster toward the scratched area. It was observed that EVs enhance cell migration under OS; thus, the scratch was filled within a day. Neither untreated nor OS-induced MSCs showed complete migration within 24 hours (Fig. 7).

### EVs Cause Upregulation of OS-Responsive Genes

NPCs showed altered gene levels of OS-responsive markers in normal, OS-induced, and EV-treated groups (Fig. 8). OS-induced NPCs revealed that *SOD1*, *SOD2*, *PRDX1*, *PRDX2*, *PRDX3*, *PRDX4*, *GPX1*, *GPX3*, and *NRF2* were significantly downregulated. However, the effect of EVs on the OS-responsive genes exhibited significant upregulation of *SOD2*, *PRDX1*, *PRDX4*, *GPX1* ( $***P < 0.001$ ),

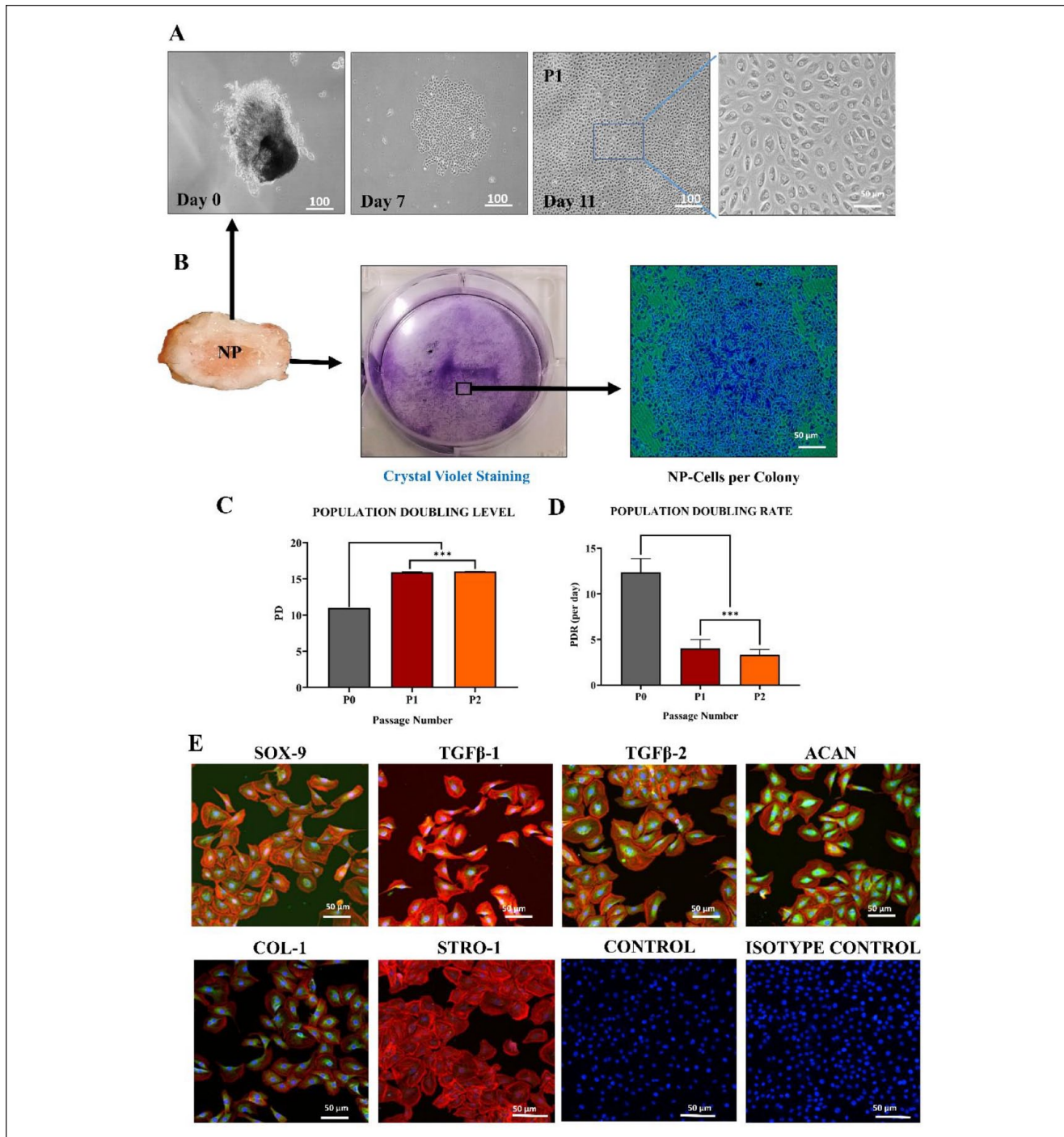


**Figure 1.** Isolation and characterization of NPCs. **(A)** Release of NPCs from NP tissue, which formed a honeycomb-like structure at day 7 of culture. NPCs reached approximately 80% confluence on the 11th day of tissue culture. The NPCs exhibited spindle-shaped morphology as the cells pass through higher passages. **(B)** Representative images of crystal violet staining of colonies formed by NPCs of different sizes and numbers. **(C, D)** Comparison between P0, P1, and P2 cells for PDL and PDR. As the number of passages increases, cells have significantly higher PDL and lower PDR. **(E)** Isolated NPCs with positive expression of chondrogenic markers SOX-9, TGFβ-1, TGFβ-2, ACAN, and COL-1, but not STRO-1, an MSC marker. Cells stained with DAPI and secondary antibodies serve only as control and isotype control, respectively. Statistical analysis was performed using an independent-sample *t* test. The data are shown as mean ± SD (*n* = 3); \*\*\* *P* < 0.001. NPCs = nucleus pulposus cells; NP = nucleus pulposus; PDL = population doubling level; PDR = population doubling rate; SOX-9 = SRY-box transcription factor 9; TGFβ-1 = transforming growth factor-beta 1; TGFβ-2 = transforming growth factor-beta 2; ACAN = aggrecan; COL-1 = collagen 1; MSCs = mesenchymal stem cells; DAPI = 4',6-diamidino-2-phenylindole.

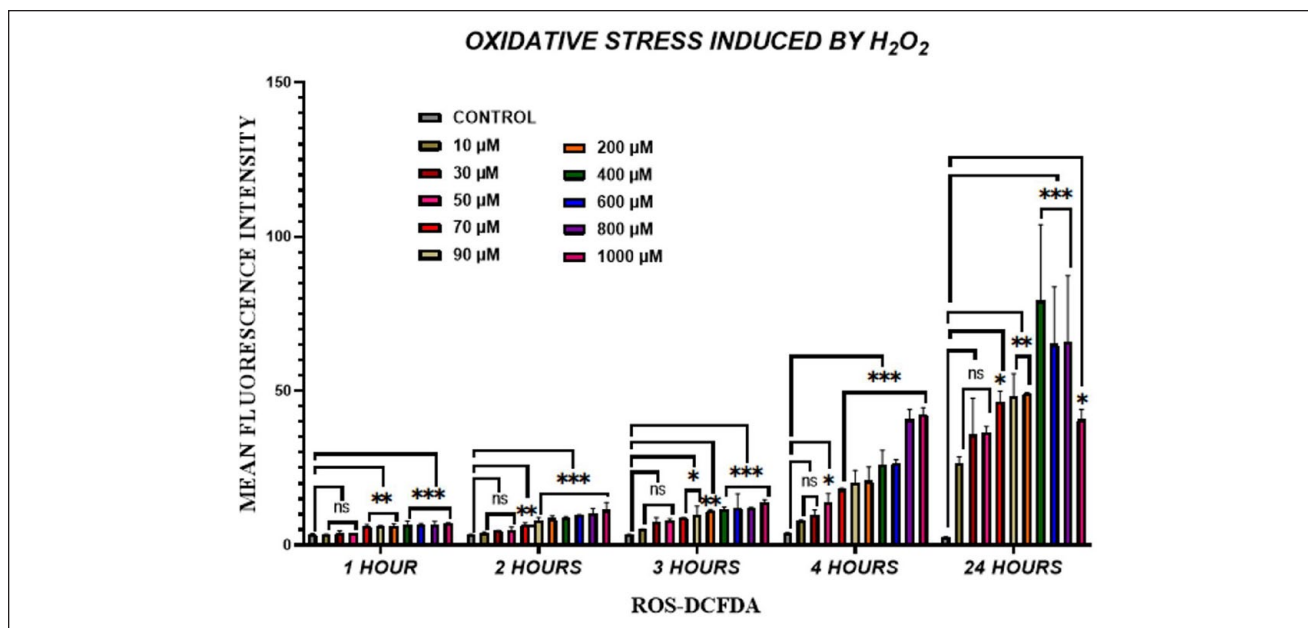


**Figure 2.** Induction of OS in NPCs. H<sub>2</sub>DCFDA assay shows concentration-dependent increase with decrease in cell viability due to ROS production and significantly less survival at 3 and 4 hours of H<sub>2</sub>O<sub>2</sub> treatment. The data are shown as mean  $\pm$  SD ( $n = 3$ ); \*\*\* $P < 0.001$ , \*\* $P < 0.01$ , and \* $P < 0.05$ . OS = oxidative stress; NPCs = nucleus pulposus cells; H<sub>2</sub>DCFDA = 2,7-dichlorofluorescein diacetate; ROS = reactive oxygen species; H<sub>2</sub>O<sub>2</sub> = hydrogen peroxide.

*SOD1*, *PRDX3*, *NRF2*, *GPX3* (\*\* $P < 0.01$ ), and *PRDX2* (\* $P < 0.05$ ).

## Discussion

IVDD is a complex multifactorial disease that causes severe degeneration of the fibrocartilage. The pathogenesis of IVDD includes an early decline in notochordal cell density of the NP, inadequate nutritional supply, and accumulation of metabolic by-products due to aging, traumatic injury, and hereditary factors.<sup>43</sup> However, the mechanism of IVDD remains unknown.<sup>44</sup> Conventional treatments for IVDD, including non-steroidal anti-inflammatory drugs (NSAIDs) and physiotherapy, are only symptomatic, whereas surgical intervention would result in several complications that could seriously impair the quality of life. As a result, it is critical to conduct research into a new therapeutic approach to treat IVDD and slow the progression of disc degeneration.

In recent years, hUC-MSCs have emerged as a unique source of MSCs for treating tissue impairment. MSCs possess reduced immunogenicity, remarkable self-renewal, and immunoregulation properties and have been reported to be well preserved in hUC-MSC-derived EV studies.<sup>45,46</sup> Lu *et al.*<sup>47</sup> demonstrated that NPC-derived EVs induced bone marrow (BM)-MSC migration and differentiation to an NP-like morphology. Also, EVs promoted NPC proliferation and restored ECM production in the degenerating

NPCs.<sup>47</sup> Studies have suggested that MSCs may play a therapeutic role *via* a paracrine mechanism.<sup>48</sup> Lan and colleagues reported that *in vitro* NPC-derived EVs induced MSC differentiation into NP-like cells by inhibiting the Notch1 pathway,<sup>49,27</sup> while Liao *et al.*<sup>50</sup> reported that endoplasmic reticulum stress reduces apoptosis by activating the ERK and AKT signaling cascade and prevents IVDD progression in a rat tail model.<sup>51</sup> According to Cheng *et al.*,<sup>52</sup> exogenous miR-21 contained in EVs prevents NPCs from undergoing apoptosis and alleviates IVDD by restraining PTEN and activating PI3K/Akt signaling in apoptotic NPCs *in vitro* and *in vivo* in a rat model.

EVs are found in many different types of cells that can deliver microRNAs to the recipient cells. Although systemic delivery of EVs is widely regarded as the most convenient method, biodistribution patterns show accumulation in the liver, spleen, and lungs. Local delivery in the NP region is regarded as a good option, especially considering the avascular nature of IVDs. In this study, we investigated the effect of EVs on OS-induced NPCs *in vitro*. We proved that EVs can protect NPCs from OS and can promote cell proliferation and migration, as well as EV uptake in cells, and upregulate OS-responsive genes while suppressing OS that may cause NPC degradation.

The explant method was used to culture rat NPCs *in vitro*. NPCs successfully adhered to the plastic surface during the early stages of primary culture. In terms of cellular morphology, the cultured rat NPCs were found to be small

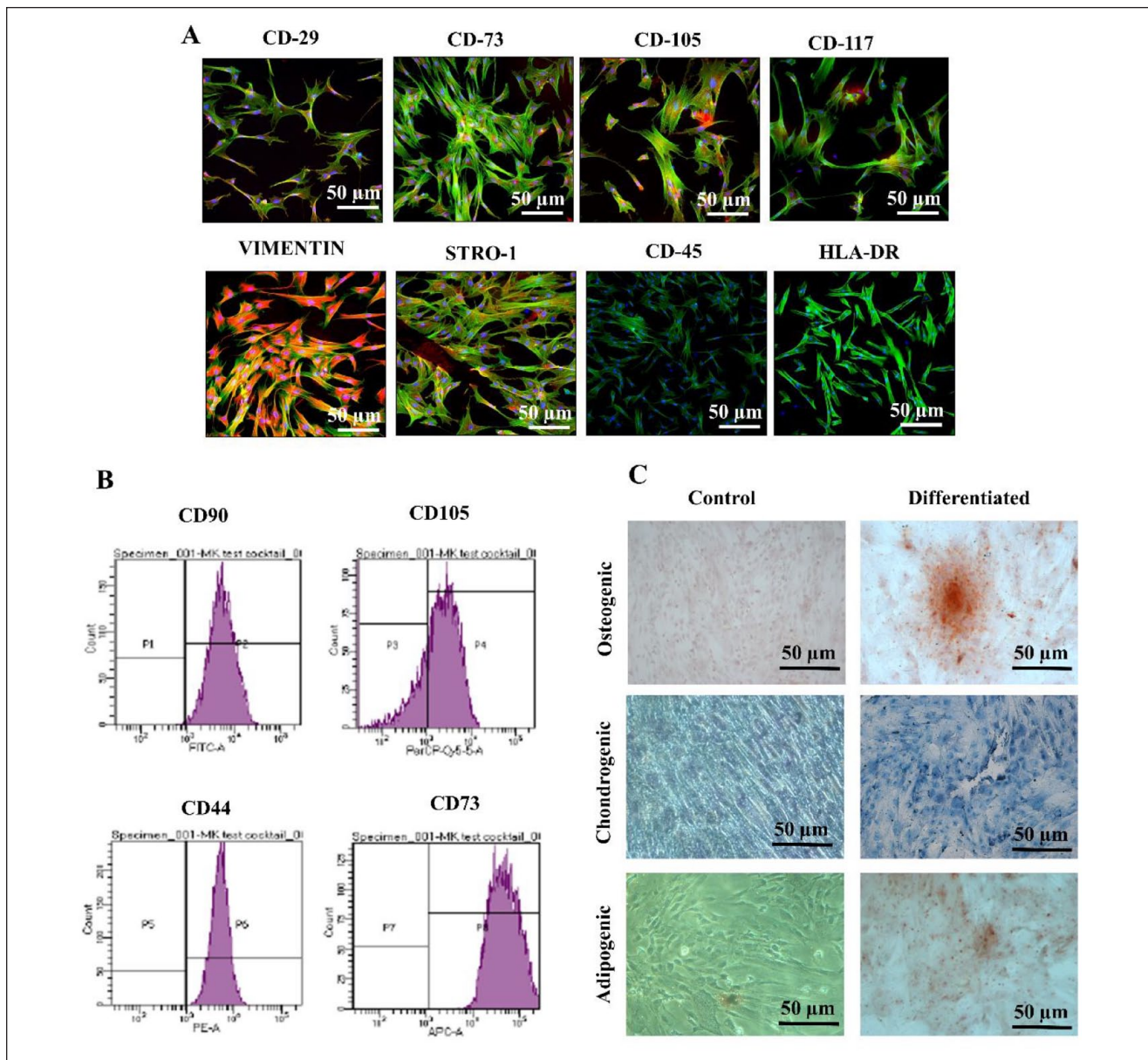


**Figure 3.** Characterizations of MSCs. **(A)** Isolated cells show positive expression of CD29, CD73, CD105, CD117, STRO-1, and vimentin and negative expression of HSC markers CD45 and HLA-DR. **(B)** Flow cytometric analysis of MSCs representing histogram peaks shows the population expressing MSC-specific markers CD90, CD105, CD44, and CD73. **(C)** Trilineage differentiation of MSCs shows positive staining with Alizarin Red S for osteocytes, Alcian Blue for chondrocytes, and Oil Red O for adipocytes. MSCs = mesenchymal stem cells. HSC = hematopoietic stem cells; HLA-DR = human leukocyte antigen-DR isotype; FITC-A = fluorescein isothiocyanate-area; PE-A = phycoerythrin-area; APC-A = allophycocyanin-area.

and spindle-shaped.<sup>36</sup> In the CFU assay, NPCs showed better colony-forming efficiency. PDL indicated that rat-derived NPCs have a higher proliferative capacity throughout the exponential phase of growth. In terms of immunophenotypic pattern, NPCs at P<sub>3</sub> expressed NP-specific markers SOX-9, TGF- $\beta$ 1, TGF- $\beta$ 2, ACAN, and COL-1, but did not express STRO-1, which is an MSC-specific marker.

The loss of NPCs has been identified as the main factor contributing to the degeneration of IVDs. Apoptosis is the primary contributor to the loss of NPCs.<sup>53,54</sup> ROS has been recognized as a by-product of mitochondrial metabolism and homeostasis.<sup>55</sup> However, excess production of ROS is a key component of increased apoptosis.<sup>27</sup> ROS has been shown to increase the degeneration of IVDs.<sup>51</sup> Therefore, we used H<sub>2</sub>O<sub>2</sub> to stimulate ROS in cells, induce cell

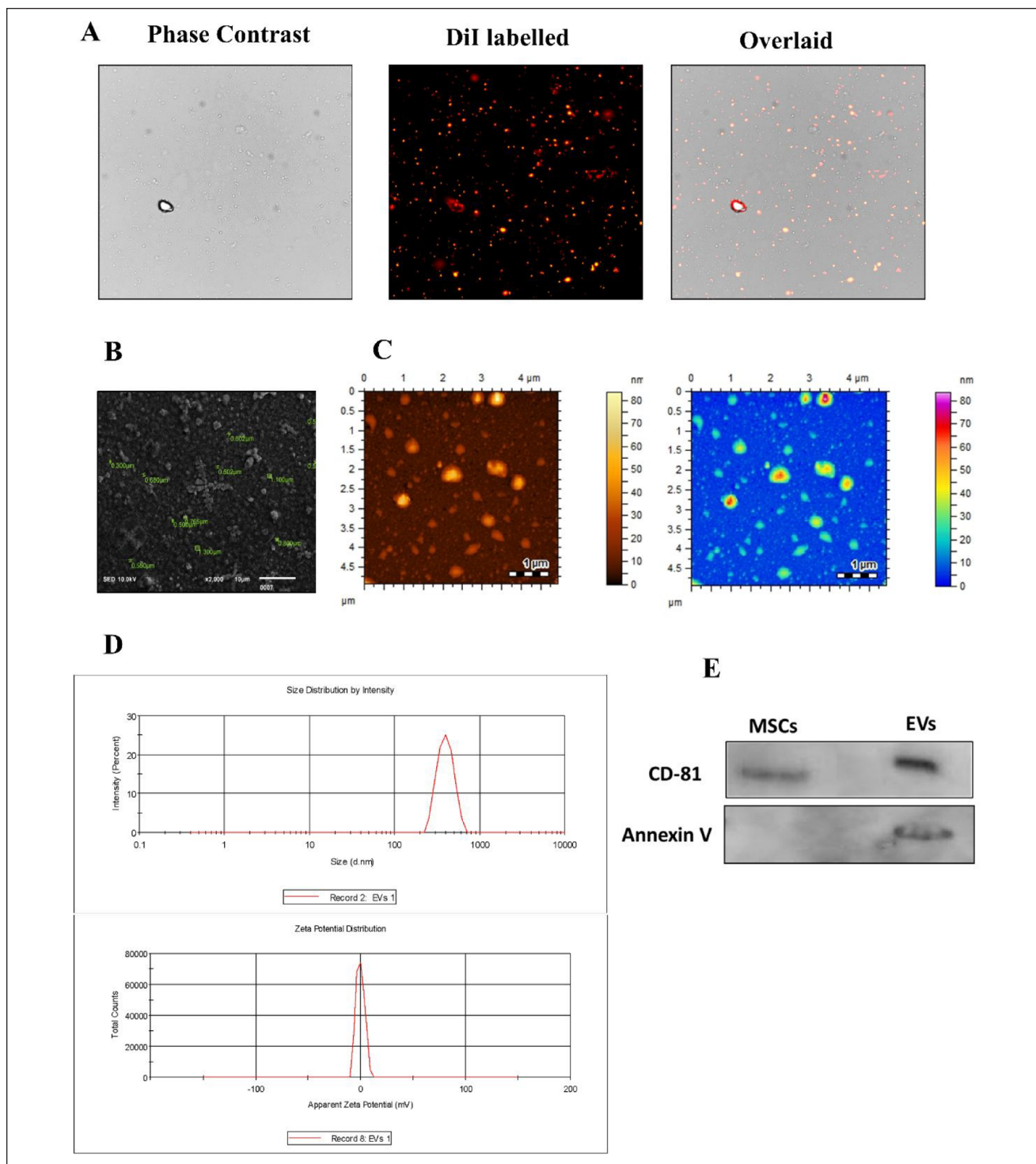


**Figure 4.** Characterization of EVs. **(A)** Distribution of EVs isolated from hUC-MSCs by differential centrifugation, evaluated by light and fluorescent microscopy. **(B)** The geometry and size of EVs by SEM. **(C)** AFM topographic 2-dimensional image (amplitude modulation) demonstrating EV adhesion to mica, drying with  $N_2$ , and capture in air. **(D)** DLS analysis using Nano Zetasizer shows the height of peak having size of EVs  $403.3 \pm 85.94$  nm, whereas zeta potential analysis shows that EVs exhibited a negative potential of about  $-0.270 \pm 4.04$  mV. Zeta potential less than zero is considered stable in an aqueous solution, and 4.04 mV indicates that EVs exhibited stable aqueous dispersion in a physiologic environment. **(E)** A total protein extract of EVs was analyzed by WB using antibodies that recognized CD81 and annexin V. EVs = extracellular vesicles; hUC-MSCs = human umbilical cord-mesenchymal stem cells; SEM = scanning electron microscope; AFM = atomic force microscope; DLS = dynamic light scattering; WB = Western blot.

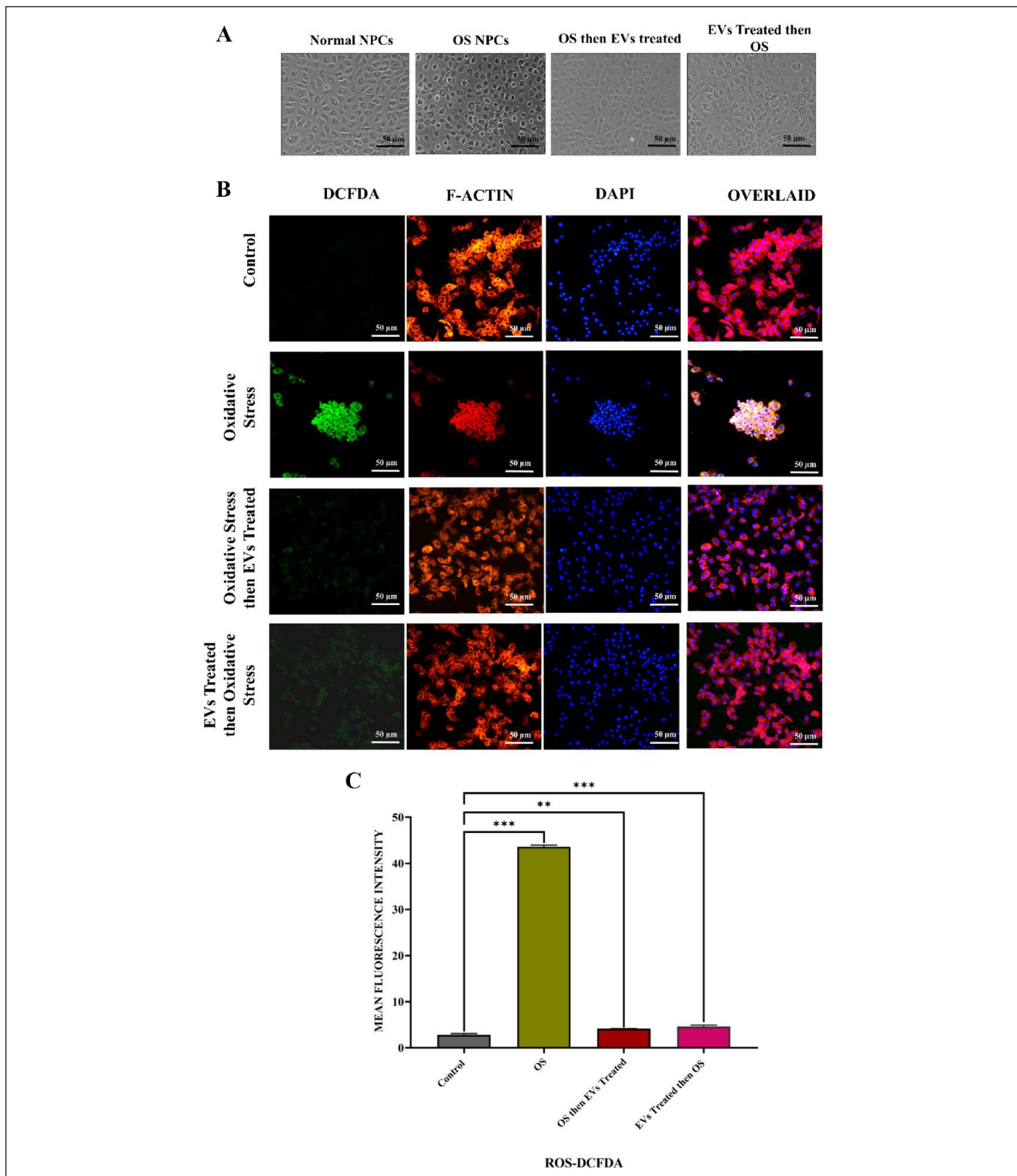


**Figure 5.** ROS level in untreated and EV-treated NPCs. **(A)** Untreated NPCs, OS-induced NPCs, OS-induced NPCs treated with EVs, and OS-induced NPCs treated with EVs and then exposed with OS. Morphological analysis was performed to evaluate the OS induced by  $H_2O_2$ . At 200  $\mu M$  concentrations, phase contrast images show that the majority of the NPCs are shrunken with a thread-like matrix, while others appeared floating in the medium. After EV treatment, there was a significant difference in morphology. **(B)** Fluorescence images of control, OS-induced NPCs, and OS-induced NPCs treated with EVs. Two-hour exposure to 200  $\mu M$   $H_2O_2$  significantly increased ROS level, while the EV treatment significantly reduced the level of ROS. **(C)** Quantification of the fluorescence intensity for ROS measurement. The data are shown as mean  $\pm$  SD ( $n = 3$ ); \*\*\* $P < 0.001$  and \*\* $P < 0.01$ . ROS = reactive oxygen species; EVs = extracellular vesicles; NPCs = nucleus pulposus cells; OS = oxidative stress;  $H_2O_2$  = hydrogen peroxide; DCFDA = dichlorofluorescein diacetate; DAPI = 4',6-diamidino-2-phenylindole.

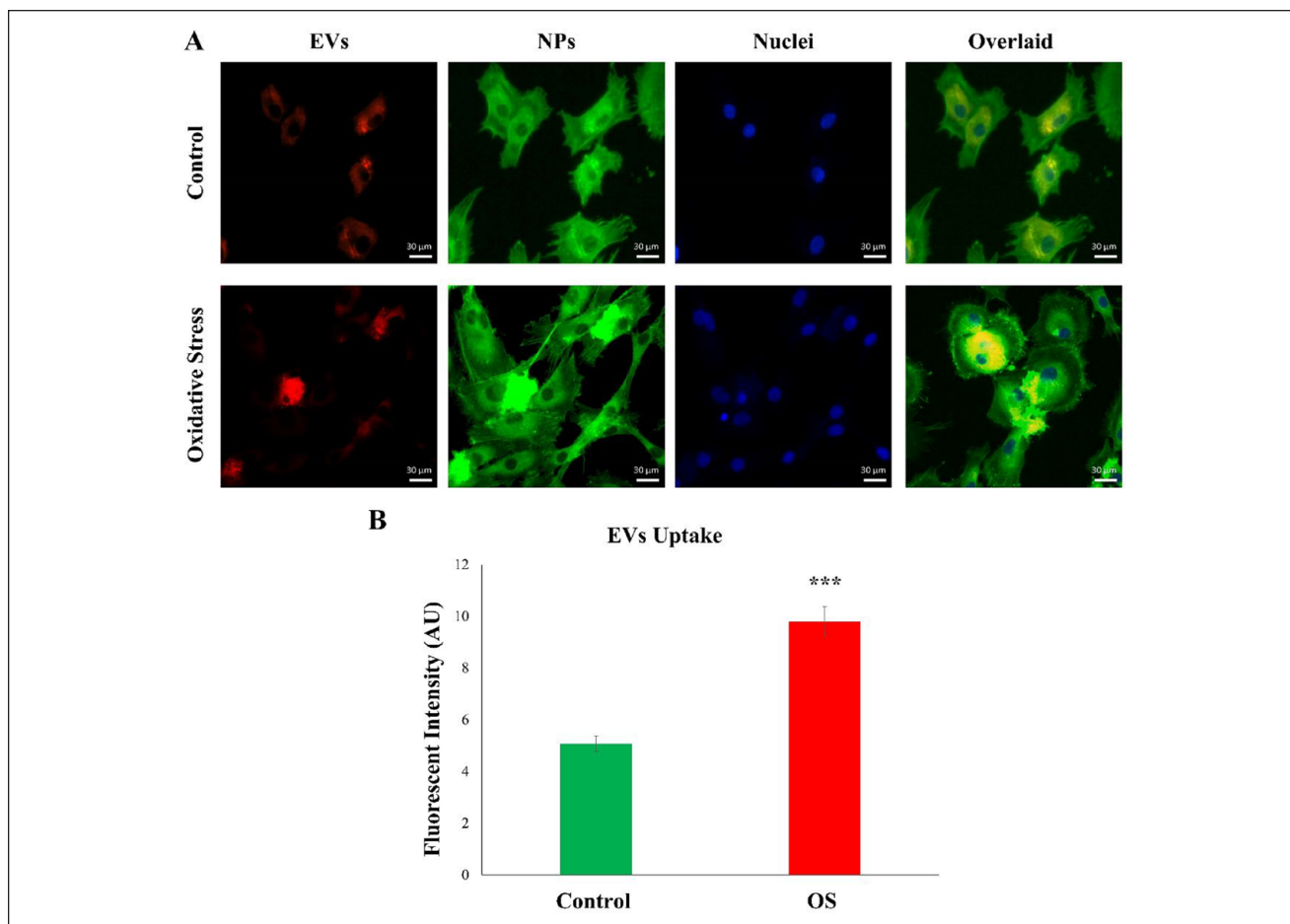


**Figure 6.** The internalization of EVs by NPCs. **(A)** Triple channel immunofluorescence analysis of Dil-stained EVs (red), F-actin (green), and DAPI (blue) in NPCs shows the presence of EVs in both control and OS-induced groups, but more in the latter. **(B)** Quantification of the fluorescence intensity for the uptake of EVs by NPCs. The data are shown as mean  $\pm$  SD ( $n = 3$ ); \*\*\* $P < 0.001$ , \*\* $P < 0.01$ , and \* $P < 0.05$ . EVs = extracellular vesicles; NPCs = nucleus pulposus cells; DAPI = 4',6-diamidino-2-phenylindole.

damage, and develop a programmed cell death model in NPCs *in vitro*.

As OS is mainly associated with the pathogenesis of IVDD, it potentially causes IVD senescence and induces autophagy and apoptosis. As a result, the proportion of functional and viable cells decreases significantly due to persistent OS. ROS affects the progression of IVDD by regulating the survival and function of IVD cells. Increased ROS levels induce OS, which stimulates signal transduction pathways in disc cells, including the nuclear factor kappa and mitogen-activated protein kinases (MAPK) pathways.<sup>56</sup> It is critical to assess the impact of EV treatment on lowering ROS levels and increasing the regenerative potential of disc cells. Our results show that OS increases in rat-derived NPCs in a concentration- and time-dependent manner. Next, optimized  $H_2O_2$  concentration (200  $\mu M$  for 2 hours) was used for further analysis. It significantly induced

OS in NPCs. Earlier studies in human and animal models have shown that OS and inflammation can cause severe apoptotic cell death in disc cells, leading to degeneration.<sup>57</sup>

Despite the advancement in stem cell treatment over the last couple of decades, apoptosis of the transplanted cells after *in vivo* implantation has emerged as a major hurdle in their use in the clinical setting. Only 1% of the transplanted cells remain viable at the site of action in the first few hours.<sup>58</sup> To overcome these obstacles, cell-free strategies for increasing the lifespan of functional and viable cells *in vivo* have been developed. We used hUC-MSC-derived EVs for this purpose, and we tested their effect on OS-induced NPCs. Our results suggest that the *in vitro*-reduced OS effects in NPCs could be due to hUC-MSC-derived EVs. EVs were isolated from conditioned or serum-free media containing hUC-MSCs. The total concentration of extracted EVs was nearly 200  $\mu g/ml$ . The

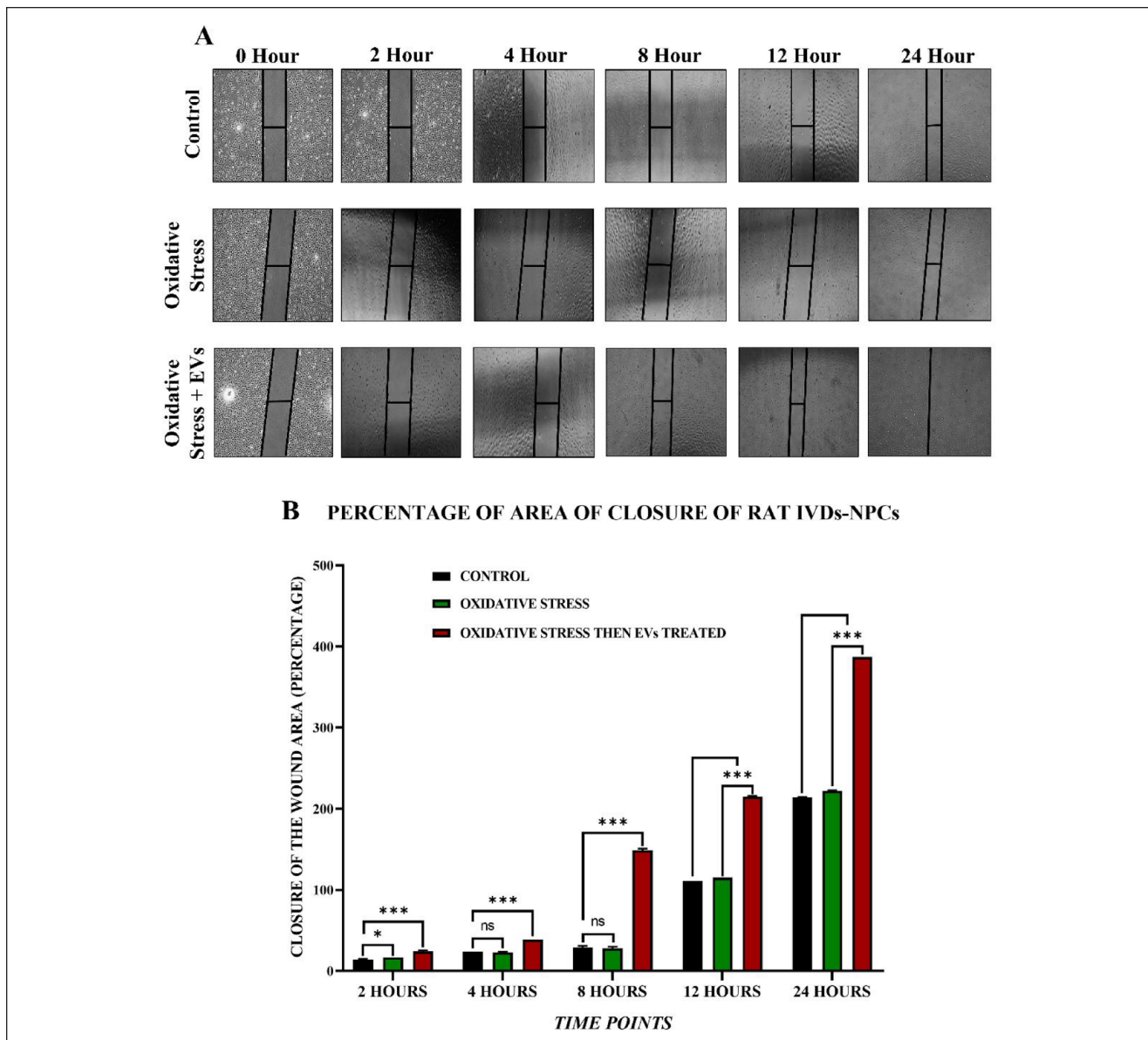


**Figure 7.** Cell migration by scratch assay. **(A)** EV-treated NPCs were subjected to OS for 24 hours following scratch. NPCs migrated at a faster rate toward the scratch, thus reducing the scratch; scratch closure was noted after 24 hours. **(B)** Quantification of scratch closure. The data are shown as mean  $\pm$  SD ( $n = 3$ );  $***P < 0.001$ ,  $*P < 0.05$ . EVs = extracellular vesicles; NPCs = nucleus pulposus cells; OS = oxidative stress.

EVs isolated from hUC-MSCs varied in size ranging from 150 to 800 nm in diameter. WB results revealed that EVs positively expressed cell surface proteins CD81 and annexin V.

OS is an imbalance between antioxidants and oxidizing agents that leads to the disruption of ROS signaling and the resulting damage. ROS remain balanced under physiological conditions and play a major role in cellular signaling and homeostasis. However, OS enhances ROS

production.<sup>56</sup> We observed that OS induction by  $H_2O_2$  significantly increases ROS levels in NPCs compared with the untreated control. The protective effect of hUC-MSC-derived EVs was also confirmed by changes in the ROS levels in both groups.

To assess the uptake of EVs derived from hUC-MSCs by the NPCs, the DiI-labeled EVs were visualized within the NPCs. Fluorescence microscopic image analysis confirmed the ability of NPCs to internalize the EVs. DiI-labeled EVs

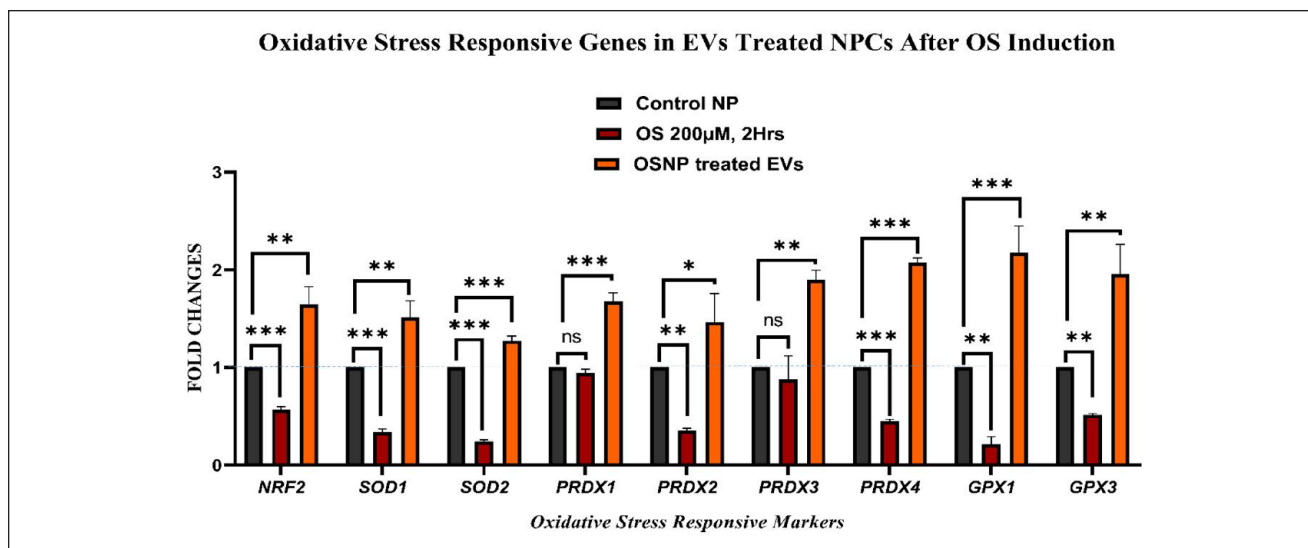


**Figure 8.** Gene expression analysis of OS markers. Twofold ( $2^{-\Delta\Delta CT}$ ) quantitative changes in *NRF2*, *PRDX1*, *PRDX2*, *PRDX3*, *PRDX4*, *SOD1*, *SOD2*, *GPX1*, and *GPX3* in NPCs, OS-induced NPCs, and EV-treated NPCs. Significant upregulation of *PRDX1*, *PRDX4*, *SOD2*, *GPX1* ( $***P < 0.001$ ), *NRF2*, *PRDX3*, *SOD1*, *GPX3* ( $**P < 0.01$ ), and *PRDX2* ( $*P < 0.05$ ) was observed in the EV-treated NPCs. The data are shown as mean  $\pm$  SD ( $n = 3$ );  $***P < 0.001$ ,  $*P < 0.05$ . OS = oxidative stress; EVs = extracellular vesicles; NPCs = nucleus pulposus cells.

were observed as an interspersed red fluorescence within the NPCs after 48 hours of incubation. It was observed that more EVs were internalized into the NPCs under OS compared with the normal NPCs. These outcomes indicate that hUC-MSC-derived EVs can be transported into NPCs, implying a possible role in the NPC and EV interaction.

The scratch assay showed that 150  $\mu\text{g/ml}$  EVs enhanced NPC migration, as the scratch was filled within 24 hours of EV treatment, which is not the case in control and OS-induced NPCs. Moreover, these NPCs were found to be populated with cell debris because of incredibly high cell proliferation having multiple cell layers indicating high expansion. It has been demonstrated that endometrial MSC-derived exosomes promote human umbilical vein endothelial cell (HUVEC) propagation, migration, and angiogenesis and significantly increase proliferative and angiogenesis markers in a dose-dependent manner.<sup>59</sup>

As NPC-derived EVs have previously been examined for their immunostimulatory and antioxidative effects,<sup>49</sup> we investigated the effect of hUC-MSC-derived EVs on NP cells. To mimic the environmental stresses that cause cell apoptosis *in vivo*, NPCs were subjected to  $\text{H}_2\text{O}_2$ -induced OS.<sup>51</sup> Despite significantly high ROS levels in OS and / or disease-related microenvironments, OS-responsive markers are highly expressed to restore stability and reduce ROS accumulation. We observed that untreated NPCs induced with  $\text{H}_2\text{O}_2$  (200  $\mu\text{M}$ , 2 hours) demonstrate low expression of OS-responsive markers, implying that the cell's antioxidative defense system is impaired. Thus, an imbalance in the ROS and antioxidative defense system causes OS. EVs

were able to prevent the accumulation of OS in the NPCs by increasing the expression level of OS-responsive markers, thereby lowering the production of ROS.

Several OS-responsive markers were analyzed. These markers were highly expressed in response to OS as a homeostasis mechanism. Expression of superoxide dismutase (*SOD*), peroxiredoxins (*PRDXs*), and glutathione peroxidases (*GPXs*) is regulated by nuclear factor-like 2 (*NRF2*). *SOD* catalyzes the reduction of superoxides to peroxides, which are then acted upon by *PRDX* and *GPX* to produce water.<sup>60</sup> Such events support the significant reduction in ROS production through hUC-MSC-derived EVs when compared with untreated NPCs under OS. However, when compared with the control group, EV-treated NPCs were able to prevent OS formation, whereas ROS levels in the EV-treated group were slightly increased. It was observed that hUC-MSC-derived EVs enhanced OS response and antioxidant gene expression in NPCs when compared with untreated NPCs and OS-induced NPCs. NPCs treated with EVs for 48 hours significantly increased the expression levels *SOD2*, *PRDX1*, *PRDX4*, *GPX1* ( $***P < 0.001$ ); *SOD1*, *PRDX3*, *NRF2*, *GPX3* ( $**P < 0.01$ ); and *PRDX2* ( $*P < 0.05$ ). It has been demonstrated that exosomes obtained from platelet-rich plasma (PRP) abundant in miR-141-3p reduce the cytotoxicity effect of  $\text{H}_2\text{O}_2$  on NP cells *via* regulating the kelch-like ECH-associated protein 1 (Keap1)/*NRF2* pathway and decrease the development of IVDD in mice.<sup>61</sup> In another study, the effect of human MSC-derived smaller EVs (sEVs) on degenerative IVD cells obtained from patients with degenerated IVDs and chronic pain was examined in a 3-dimensional *in vitro*

model. The results showed that sEV therapy displayed greater than 50% rise in cellular proliferation and reduced cell apoptosis in degenerating IVD cells. Furthermore, sEV therapy reduced *matrix metalloproteinase-1* (MMP-1) release in IVD cells.

### Limitations of the Study

Further investigation is required to analyze the molecular mechanisms underlying H<sub>2</sub>O<sub>2</sub>-induced OS, which may aid in the development of strategies to prevent IVD-related degenerative diseases using cell therapy approaches. Additional research based on *in vivo* preclinical and clinical studies of EVs is required to develop an effective cell-free therapy for IVD.

### Conclusion

In conclusion, the findings of this study demonstrate that hUC-MSC-derived EVs have an antioxidative effect on OS-induced NPCs *in vitro*. EVs inhibit intracellular ROS generation, protecting NPCs from apoptosis, promoting NPC proliferation, and increasing EV uptake by NPCs. An increase in the expression level of OS-responsive genes was observed following EV treatment. EVs could play an important role in the intrinsic repair mechanism of IVD as a cell-free therapeutic approach for IVDD. Furthermore, EVs, because of their diverse functions, can also be used as vehicles for genes and drugs and open new therapeutic avenues for the use of EVs for the treatment of IVDD.

### Acknowledgment and Funding

This study was supported by higher education commission Pakistan, NRPUR grant # 7083.

### Declaration of Conflicting Interests

The author(s) declared no potential conflicts of interest with respect to the research, authorship, and/or publication of this article.

### Ethical Approval

This study was approved by the institutional animal care and use committee authorization no. 2017-0051.

### ORCID iD

Irfan Khan  <https://orcid.org/0000-0003-1878-7836>

### References

- Wiklander OP, Nordin JZ, O'Loughlin A, Gustafsson Y, Corso G, Mäger I, *et al.* Extracellular vesicle *in vivo* biodistribution is determined by cell source, route of administration and targeting. *J Extracell Vesicles*. 2015;4(1):26316.
- Claridge B, Lozano J, Poh QH, Greening DW. Development of extracellular vesicle therapeutics: challenges, considerations, and opportunities. *Front Cell Dev Biol*. 2021;9:734720.
- Zhang W, Jiang H, Kong Y. Exosomes derived from platelet-rich plasma activate YAP and promote the fibrogenic activity of Müller cells via the PI3K/Akt pathway. *Exp Eye Res*. 2020;193:107973.
- Ermakov KV, Bukhvostov AA, Vedenkin AS, Stovbun SV, Dvornikov AS, Kuznetsov DA. Ultrashort ssDNA in retinoblastoma patients blood plasma detected by a novel high resolution HPCL technique: a preliminary report. *Acta Medica*. 2020;62(4):170-3.
- Tracy SA, Ahmed A, Tigges JC, Ericsson M, Pal AK, Zurakowski D, *et al.* A comparison of clinically relevant sources of mesenchymal stem cell-derived exosomes: bone marrow and amniotic fluid. *J Pediatr Surg*. 2019;54(1):86-90.
- Domenis R, Zanutel R, Caponnetto F, Toffoletto B, Cifù A, Pistis C, *et al.* Characterization of the proinflammatory profile of synovial fluid-derived exosomes of patients with osteoarthritis. *Mediators Inflamm*. 2017;2017:4814987.
- Yamamoto S, Okamura K, Fujii R, Kawano T, Ueda K, Yajima Y, *et al.* Specimen-specific drift of densities defines distinct subclasses of extracellular vesicles from human whole saliva. *PLoS ONE*. 2021;16(4):e0249526.
- Chung IM, Rajakumar G, Venkidasamy B, Subramanian U, Thiruvengadam M. Exosomes: current use and future applications. *Clinica Chimica Acta*. 2020;500:226-32.
- EL Andaloussi S, Mäger I, Breakefield XO, Wood MJ. Extracellular vesicles: biology and emerging therapeutic opportunities. *Nat Rev Drug Discov*. 2013;12(5):347-57.
- Théry C, Amigorena S, Raposo G, Clayton A. Isolation and characterization of exosomes from cell culture supernatants and biological fluids. *Curr Protoc Cell Biol*. 2006;30(1):3-22.
- Mashouri L, Yousefi H, Aref AR, Molaei F, Alahari SK. Exosomes: composition, biogenesis, and mechanisms in cancer metastasis and drug resistance. *Molecular Cancer*. 2019;18(1):1-4.
- Skotland T, Hessvik NP, Sandvig K, Llorente A. Thematic review series: exosomes and microvesicles: lipids as key components of their biogenesis and functions: exosomal lipid composition and the role of ether lipids and phosphoinositides in exosome biology. *J Lipid Res*. 2019;60(1):9.
- Winczura K, Domanski M, LaCava J. Affinity proteomic analysis of the human exosome and its cofactor complexes. *Methods Mol Biol*. 2020;2062:291-325.
- Conigliaro A, Fontana S, Raimondo S, Alessandro R. Exosomes: nanocarriers of biological messages. *Adv Exp Med Biol*. 2017;998:23-43.
- Liu W, Rong Y, Wang J, Zhou Z, Ge X, Ji C, *et al.* Exosome-shuttled miR-216a-5p from hypoxic preconditioned mesenchymal stem cells repair traumatic spinal cord injury by shifting microglial M1/M2 polarization. *J Neuroinflammation*. 2020;17(1):47.
- Shyu KG, Wang BW, Pan CM, Fang WJ, Lin CM. Hyperbaric oxygen boosts long noncoding RNA MALAT1 exosome secretion to suppress microRNA-92a expression in therapeutic angiogenesis. *Int J Cardiol*. 2019;274:271-8.
- Khorkova O, Hsiao J, Wahlestedt C. Basic biology and therapeutic implications of lncRNA. *Adv Drug Deliv Rev*. 2015;87:15-24.

18. Wei Z, Batagov AO, Schinelli S, Wang J, Wang Y, El Fatimy R, *et al.* Coding and noncoding landscape of extracellular RNA released by human glioma stem cells. *Nature Communications*. 2017;8(1):1145.
19. Luan X, Sansanaphongpricha K, Myers I, Chen H, Yuan H, Sun D. Engineering exosomes as refined biological nanoplatforms for drug delivery. *Acta Pharmacol Sin*. 2017;38(6):754-63.
20. Chan WC, Sze KL, Samartzis D, Leung VY, Chan D. Structure and biology of the intervertebral disk in health and disease. *Orthop Clin North Am*. 2011;42(4):447-64.
21. Hunter CJ, Matyas JR, Duncan NA. The three-dimensional architecture of the notochordal nucleus pulposus: novel observations on cell structures in the canine intervertebral disc. *J Anat*. 2003;202(Pt. 3):279-91.
22. Risbud MV, Shapiro IM. Notochordal cells in the adult intervertebral disc: new perspective on an old question. *Crit Rev Eukaryot Gene Expr*. 2011;21(1):29-41.
23. Urban JP, Roberts S. Degeneration of the intervertebral disc. *Arthritis Res Ther*. 2003;5(3):120-30.
24. Katz JN. Lumbar disc disorders and low-back pain: socioeconomic factors and consequences. *J Bone Joint Surg Am*. 2006;88(Suppl. 2):21-4.
25. Teraguchi M, Yoshimura N, Hashizume H, Muraki S, Yamada H, Minamide A, *et al.* Prevalence and distribution of intervertebral disc degeneration over the entire spine in a population-based cohort: the Wakayama Spine Study. *Osteoarthritis Cartilage*. 2014;22(1):104-10.
26. Du J, Pfannkuche JJ, Lang G, Häckel S, Creemers LB, Alini M, *et al.* Proinflammatory intervertebral disc cell and organ culture models induced by tumor necrosis factor alpha. *JOR Spine*. 2020;3(3):e1104.
27. Suzuki S, Fujita N, Hosogane N, Watanabe K, Ishii K, Toyama Y, *et al.* Excessive reactive oxygen species are therapeutic targets for intervertebral disc degeneration. *Arthritis Res Ther*. 2015;17:316.
28. Zhang T, Wang Y, Li R, Xin J, Zheng Z, Zhang X, *et al.* ROS-responsive magnesium-containing microspheres for antioxidative treatment of intervertebral disc degeneration. *Acta Biomater*. 2023;158:475-92.
29. Song Y, Lu S, Geng W, Feng X, Luo R, Li G, *et al.* Mitochondrial quality control in intervertebral disc degeneration. *Exp Mol Med*. 2021;53(7):1124-33.
30. Li D, Tao F, Jin L. Mitochondrial dysfunction in intervertebral disc degeneration: from pathogenesis to therapeutic target. *Oxidative Med Cell Longev*. 2020;2020:1-13.
31. Ma KG, Shao ZW, Yang SH, Wang J, Wang BC, Xiong LM, *et al.* Autophagy is activated in compression-induced cell degeneration and is mediated by reactive oxygen species in nucleus pulposus cells exposed to compression. *Osteoarthritis and Cartilage*. 2013;21(12):2030-8.
32. Krut Z, Pelled G, Gazit D, Gazit Z. Stem cells and exosomes: new therapies for intervertebral disc degeneration. *Cells*. 2021;10(9):2241.
33. Noriega DC, Ardura F, Hernández-Ramajo R, Martín-Ferrero MÁ, Sánchez-Lite I, Toribio B, *et al.* Intervertebral disc repair by allogeneic mesenchymal bone marrow cells: a randomized controlled trial. *Transplantation*. 2017;101(8):1945-51.
34. Zhang J, Zhang J, Zhang Y, Liu W, Ni W, Huang X, *et al.* Mesenchymal stem cells-derived exosomes ameliorate intervertebral disc degeneration through inhibiting pyroptosis. *J Cell Mol Med*. 2020;24(20):11742-54.
35. Einabadi M, Ai J, Kargar M, Kafilzadeh F, Taghdiri Nooshabadi V, Jamali H. Mesenchymal cell-derived exosomes as novel useful candidates for drug delivery. *Arch Neurosci*. 2020;7(2):e98722.
36. Risbud MV, Guttapalli A, Stokes DG, Hawkins D, Danielson KG, Schaer TP, *et al.* Nucleus pulposus cells express HIF-1 $\alpha$  under normoxic culture conditions: a metabolic adaptation to the intervertebral disc microenvironment. *J Cell Biochem*. 2006;98(1):152-9.
37. Ekram S, Khalid S, Bashir I, Salim A, Khan I. Human umbilical cord-derived mesenchymal stem cells and their chondroprogenitor derivatives reduced pain and inflammation signaling and promote regeneration in a rat intervertebral disc degeneration model. *Mol Cell Biochem*. 2021;476(8):3191-205.
38. Zhang J, Wang JH. Characterization of differential properties of rabbit tendon stem cells and tenocytes. *BMC Musculoskelet Disord*. 2010;11:10.
39. Cristofalo VJ, Allen RG, Pignolo RJ, Martin BG, Beck JC. Relationship between donor age and the replicative lifespan of human cells in culture: a reevaluation. *Proc Natl Acad Sci USA*. 1998;95(18):10614-9.
40. Kaji K, Matsuo M. Aging of chick embryo fibroblasts in vitro-I. Saturation density and population doubling rate. *Exp Gerontol*. 1978;13(6):439-45.
41. Konoshenko MY, Lekchnov EA, Vlassov AV, Laktionov PP. Isolation of extracellular vesicles: general methodologies and latest trends. *Biomed Res Int*. 2018;2018:8545347.
42. Zhang B, Shen L, Shi H, Pan Z, Wu L, Yan Y, *et al.* Exosomes from human umbilical cord mesenchymal stem cells: identification, purification, and biological characteristics. *Stem Cells Int*. 2016;2016:1929536.
43. Urban JP, Smith S, Fairbank JC. Nutrition of the intervertebral disc. *Spine*. 2004;29(23):2700-9.
44. Wong AYL, Karppinen J, Samartzis D. Low back pain in older adults: risk factors, management options and future directions. *Scoliosis Spinal Disord*. 2017;12:14-23.
45. Fuloria S, Subramaniyan V, Dahiya R, Dahiya S, Sudhakar K, Kumari U, *et al.* Mesenchymal stem cell-derived extracellular vesicles: regenerative potential and challenges. *Biology*. 2021;10(3):172.
46. Shao M, Xu Q, Wu Z, Chen Y, Shu Y, Cao X, *et al.* Exosomes derived from human umbilical cord mesenchymal stem cells ameliorate IL-6-induced acute liver injury through miR-455-3p. *Stem Cell Res Ther*. 2020;11(1):37.
47. Lu K, Li HY, Yang K, Wu JL, Cai XW, Zhou Y, *et al.* Exosomes as potential alternatives to stem cell therapy for intervertebral disc degeneration: in-vitro study on exosomes in interaction of nucleus pulposus cells and bone marrow mesenchymal stem cells. *Stem Cell Res Ther*. 2017;8(1):108.
48. Maacha S, Sidahmed H, Jacob S, Gentilcore G, Calzone R, Grivel JC, *et al.* Paracrine mechanisms of mesenchy-

- mal stromal cells in angiogenesis. *Stem Cells Int.* 2020;2020:4356359.
49. Lan WR, Pan S, Li HY, Sun C, Chang X, Lu K, *et al.* Inhibition of the Notch1 pathway promotes the effects of nucleus pulposus cell-derived exosomes on the differentiation of mesenchymal stem cells into nucleus pulposus-like cells in rats. *Stem Cells Int.* 2019;2019:8404168.
  50. Liao Z, Luo R, Li G, Song Y, Zhan S, Zhao K, *et al.* Exosomes from mesenchymal stem cells modulate endoplasmic reticulum stress to protect against nucleus pulposus cell death and ameliorate intervertebral disc degeneration in vivo. *Theranostics.* 2019;9(14):4084-100.
  51. Chen JW, Ni BB, Li B, Yang YH, Jiang SD, Jiang LS. The responses of autophagy and apoptosis to oxidative stress in nucleus pulposus cells: implications for disc degeneration. *Cell Physiol Biochem.* 2014;34(4):1175-89.
  52. Cheng X, Zhang G, Zhang L, Hu Y, Zhang K, Sun X, *et al.* Mesenchymal stem cells deliver exogenous miR-21 via exosomes to inhibit nucleus pulposus cell apoptosis and reduce intervertebral disc degeneration. *J Cell Mol Med.* 2018;22(1):261-76.
  53. Vo NV, Hartman RA, Patil PR, Risbud MV, Kletsas D, Iatridis JC, *et al.* Molecular mechanisms of biological aging in intervertebral discs. *J Orthop Res.* 2016;34(8):1289-306.
  54. Wang F, Cai F, Shi R, Wang XH, Wu XT. Aging and age related stresses: a senescence mechanism of intervertebral disc degeneration. *Osteoarthritis Cartilage.* 2016;24(3):398-408.
  55. Zorov DB, Juhaszova M, Sollott SJ. Mitochondrial reactive oxygen species (ROS) and ROS-induced ROS release. *Physiological Reviews.* 2014;94(3):909-50.
  56. Feng C, Yang M, Lan M, Liu C, Zhang Y, Huang B, *et al.* ROS: crucial intermediators in the pathogenesis of intervertebral disc degeneration. *Oxidative Med Cell Longev.* 2017;2017:5601593.
  57. Rider SM, Mizuno S, Kang JD. Molecular mechanisms of intervertebral disc degeneration. *Spine Surg Relat Res.* 2018;3(1):1-11.
  58. Baldari S, Di Rocco G, Piccoli M, Pozzobon M, Muraca M, Toietta G. Challenges and strategies for improving the regenerative effects of mesenchymal stromal cell-based therapies. *Int J Mol Sci.* 2017;18(10):2087.
  59. Taghdiri Nooshabadi V, Verdi J, Ebrahimi-Barough S, Mowla J, Atlasi MA, Mazoochi T, *et al.* Endometrial mesenchymal stem cell-derived exosome promote endothelial cell angiogenesis in a dose-dependent manner: a new perspective on regenerative medicine and cell-free therapy. *Arch Neurosci.* 2019;6(4):e94041.
  60. Nie P, Bai X, Lou Y, Zhu Y, Jiang S, Zhang L, *et al.* Human umbilical cord mesenchymal stem cells reduce oxidative damage and apoptosis in diabetic nephropathy by activating Nrf2. *Stem Cell Res Ther.* 2021;12(1):450.
  61. Xu J, Xie G, Yang W, Wang W, Zuo Z, Wang W. Platelet-rich plasma attenuates intervertebral disc degeneration via delivering miR-141-3p-containing exosomes. *Cell Cycle.* 2021;20(15):1487-99.